Supporting information of

Morphology controllable nano-sheet polypyrrole/graphene composites for high-rate supercapacitor

Jianbo Zhu [a], *Youlong Xu* [a*], *Jie Wang* [a], *Jingping Wang* [b], *Yang Bai* [a], *Xianfeng Du* [a]

a Electronic Materials Research Laboratory, Key Laboratory of the Ministry of Education & International Center for Dielectric Research, Xi'an Jiaotong University

Telephone/ Fax numbers: 0086-29-82665161/0086-29-82665161; E-mail: ylxu@mail.xjtu.edu.cn

b College of chemistry and chemical engineering, Shaanxi University of Science and Technology, Xi'an 710021, China

1.The fabrication of supercapcitor by two-electrode cells system

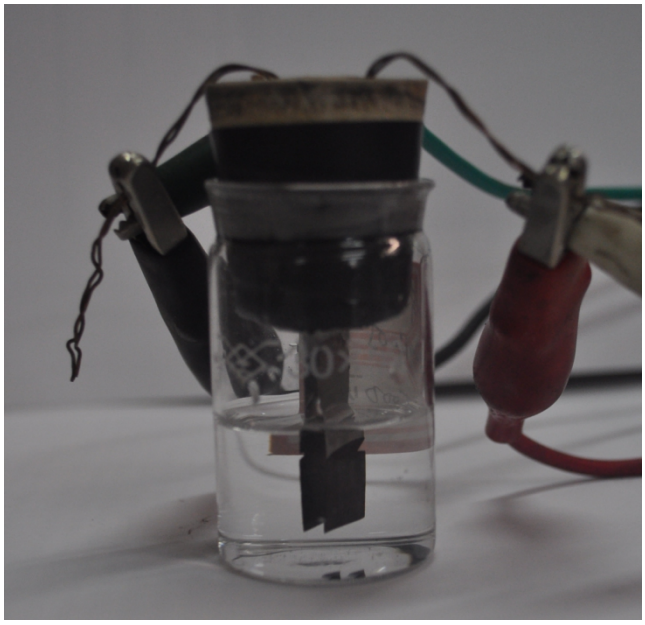

Fig. S1 a photograph of the fabricated supercapacitor, and the distance between two electrodes was about 2 mm.

2. The micelle particle size distribution of pyrrole monomers and the influence of reduced graphene oxide adding

Pyrrole (Py) monomer is a lipophilic molecule and can been dispersed in aqueous solution by forming micelles. With reduced graphene oxide (RGO) adding, the micellar size is changed significantly because of the hydrophobic interaction between hydrocarbon chains of RGO and pyrrole monomers. In the work, we prepared six aqueous suspension samples of different components (shown in Table S1) to investigative their micelle particle size distribution by the Zetasizer Nano instrument. Figure S2 and S3 show the number particle size distribution and the average grain size of each sample. As shown in Figure S2, pure Py in aqueous solution can form micelles with size about 3.7 nm, and the dopant ions TOS^- also play a role in surfactant to facilitate the formation of large-scale micelles (about 60 nm). On the other hand, with the adding of RGO, the size analysis (Fig. S3) shows that majority of size classes are located at about 500 nm which is correspond to the RGO scale. The micelle only forming by Py monomer and surfactant TOS^- is reduce or even disappear with the increasing of RGO. Such trends indicate that Py monomer is more easily absorbing onto RGO surfaces, which imply that Py monomer and RGO can form stable adsorption during the polymerization process.

Table S1 Components and average size parameters of the samples

component	Py monomer (mol L^{-1})	TOSH (mol L^{-1})	RGO (mg ml^{-1})
Sample 1	0.1	0	0
Sample 2	0.1	0.1	0
Sample 3	0.1	0.1	0.05
Sample 4	0.1	0.1	0.1
Sample 5	0.1	0	0.1
Sample 6	0	0	0.1

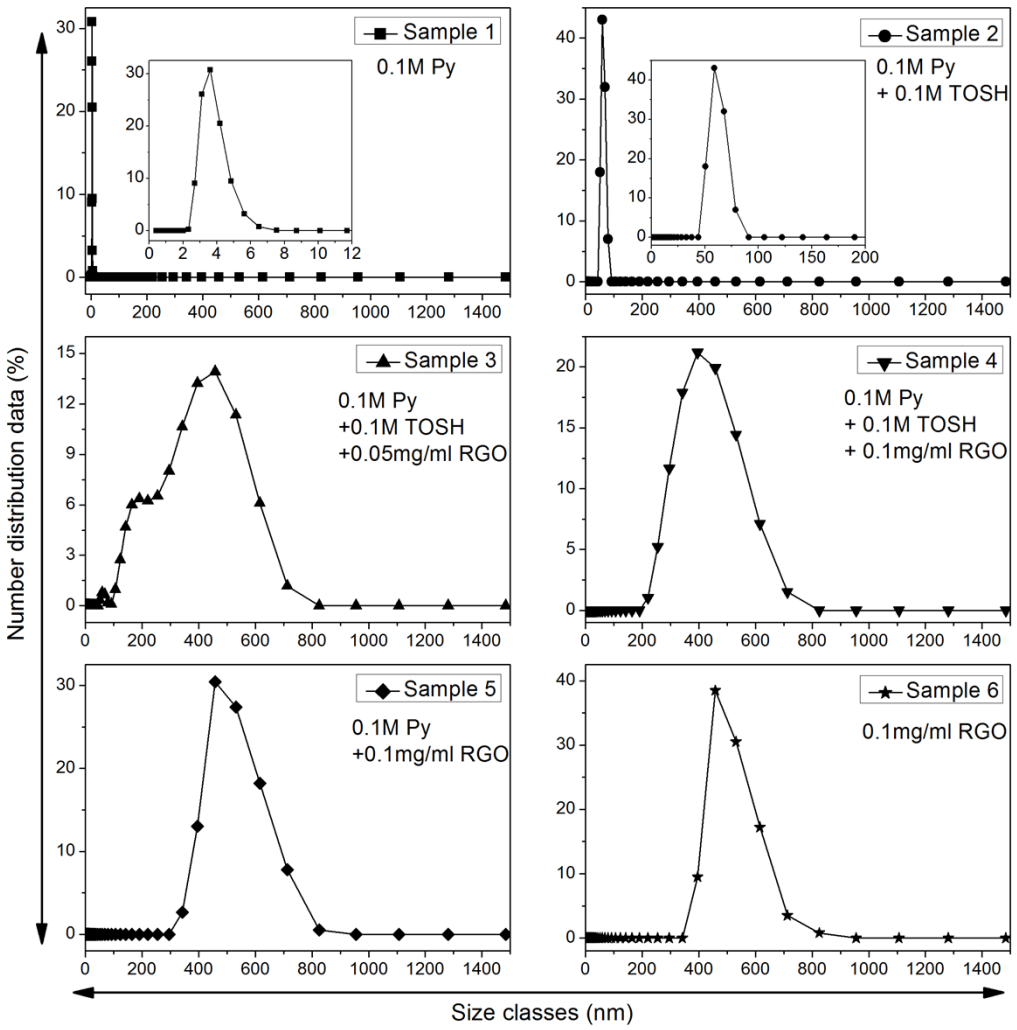

Fig. S2 Particle size distribution of the aqueous suspension sample of different component.

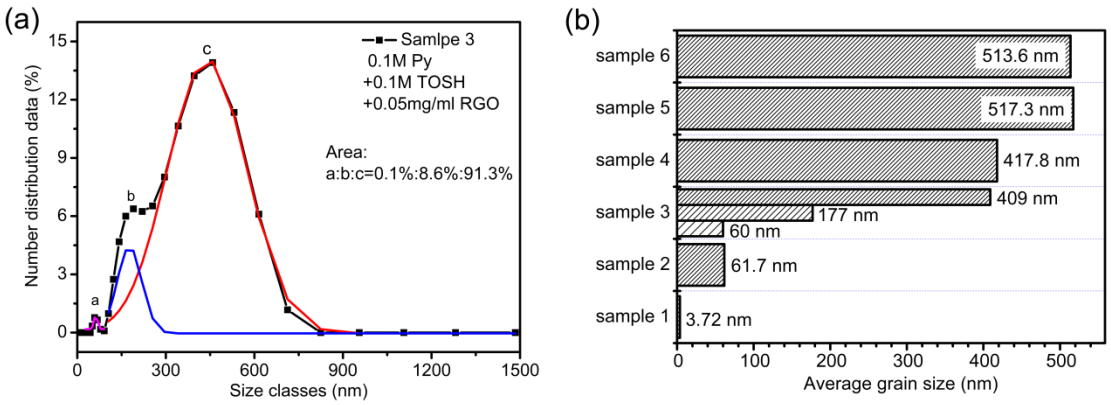

Fig. S3 (a) peaks fitting of the particle size distribution of the sample 3, and (b) average grain size of all samples.

4. Nano-size of PPy particles and PPy/RGO-10 sheets

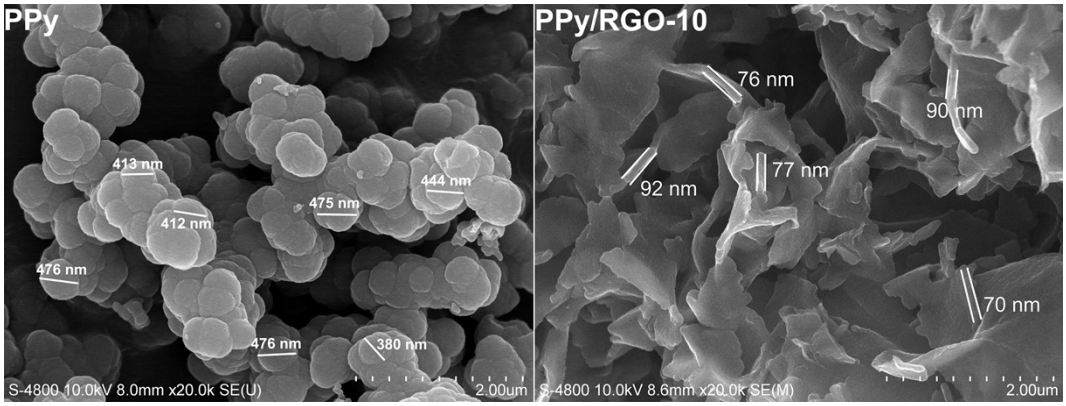

Fig. S4 SEM images and the size sign of PPy and PPy/RGO-10.

5. EDS and elemental mapping analysis

The distribution of nitrogen and sulfur elements in the PPy/RGO composites can be verified by EDS elemental mapping (Fig. S4-S9). Corresponding element mapping images indicate the presence of the presence of C, N, O, and S elements in the PPy/RGO composites, and the data of element contents are listed in table S2. The N and S distribution in the plane of nano-sheet PPy/RGO is highly homogeneous, which can further demonstrate the successful formation of composites with PPy coating on graphene.

Table S2 Atomic contents of C, N, O, and S in the different samples.

Sample	Element contents (at.%)				
	C	N	O	S	Al
RGO	72.11	--	26.53	0.45	0.91
PPy	70.2	11.06	13.95	2.89	1.9
PPy/RGO-2.5	63.21	13.96	19.40	1.73	1.7
PPyRGO-5	69.36	11.77	15.17	2.52	1.18
PPy/RGO-10	66.71	12.82	16.67	1.93	1.87
PPy/RGO-20	68.45	10.98	15.96	3.48	1.13

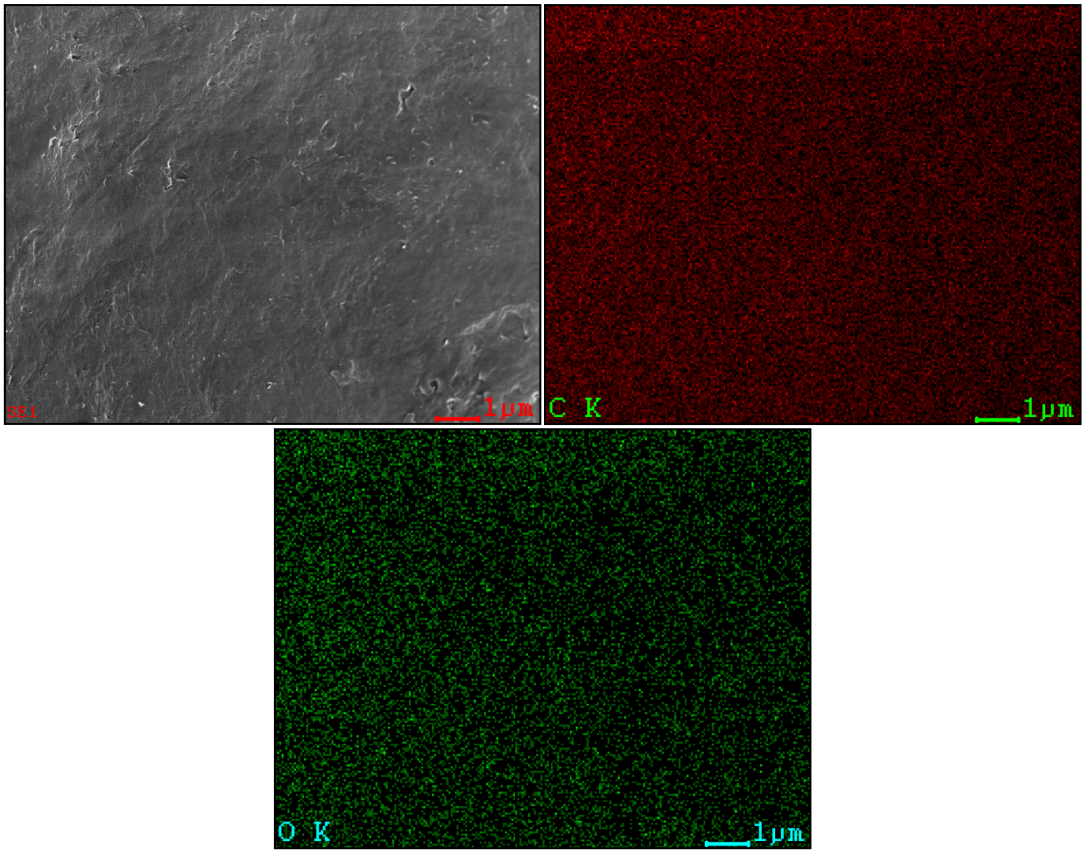

Fig. S5 SEM image of RGO and the corresponding elemental mapping images for each element.

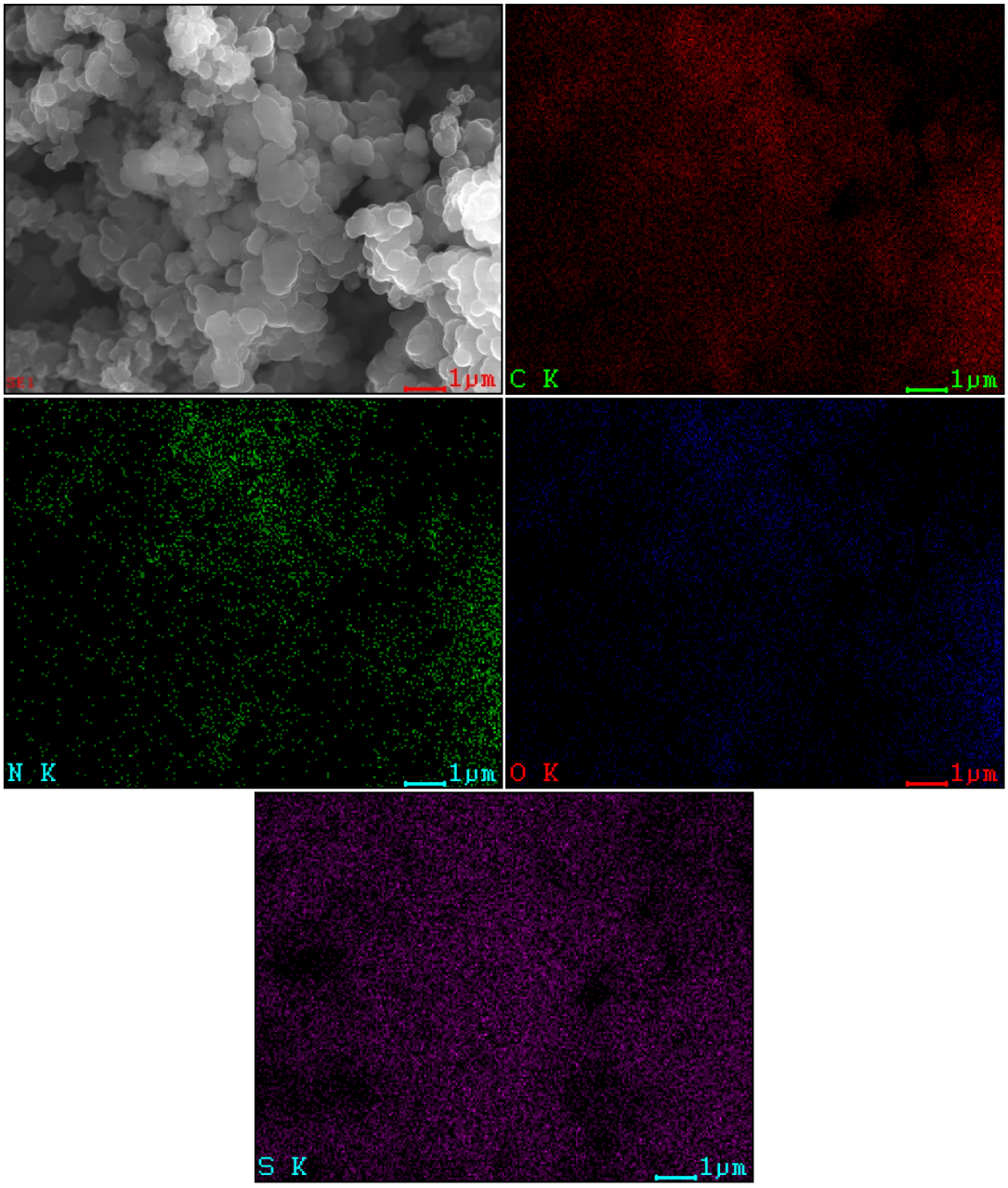

Fig. S6 SEM image of PPy and the corresponding elemental mapping images for each element.

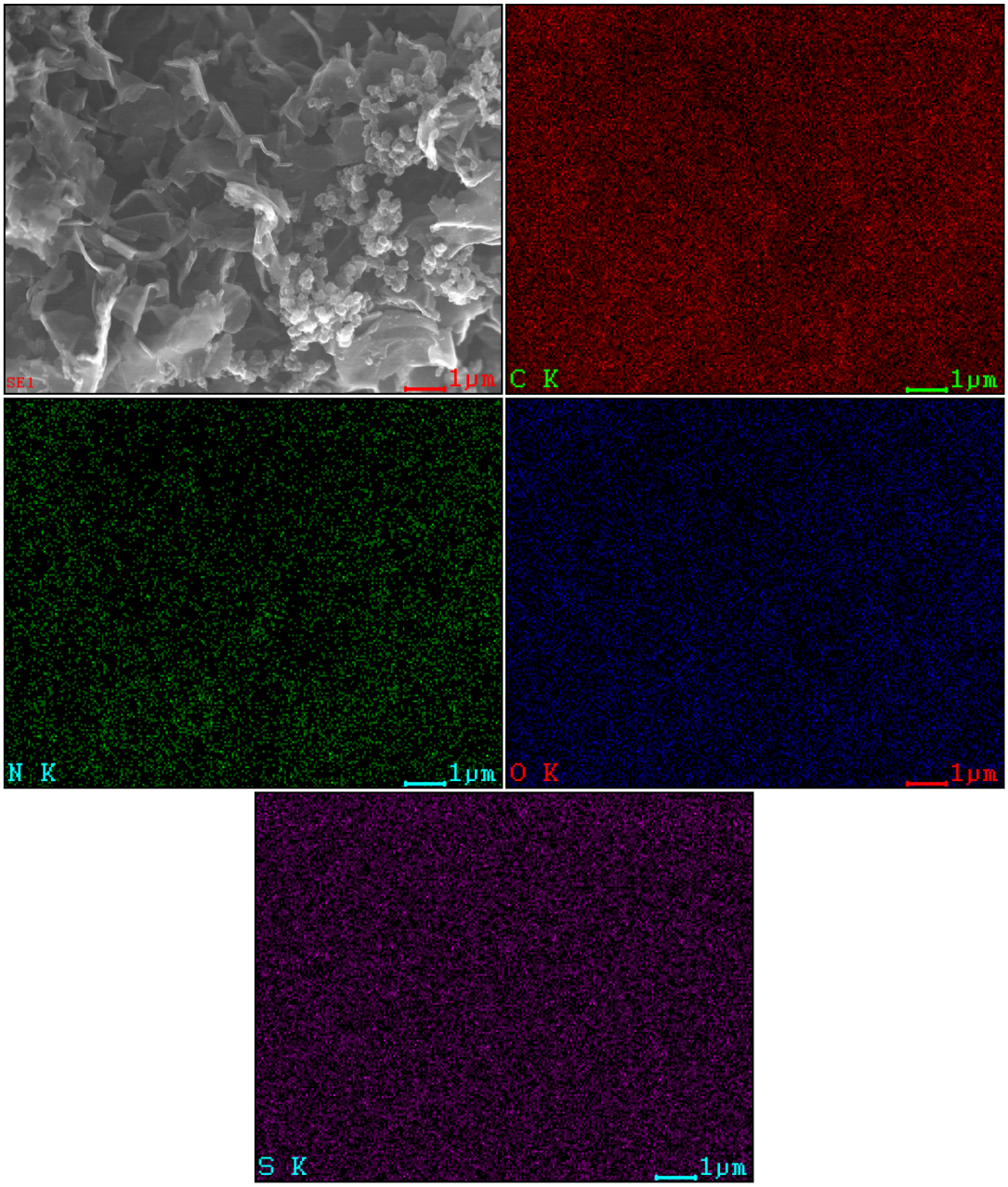

Fig. S7 SEM image of PPy/RGO-2.5 and the corresponding elemental mapping images for each element.

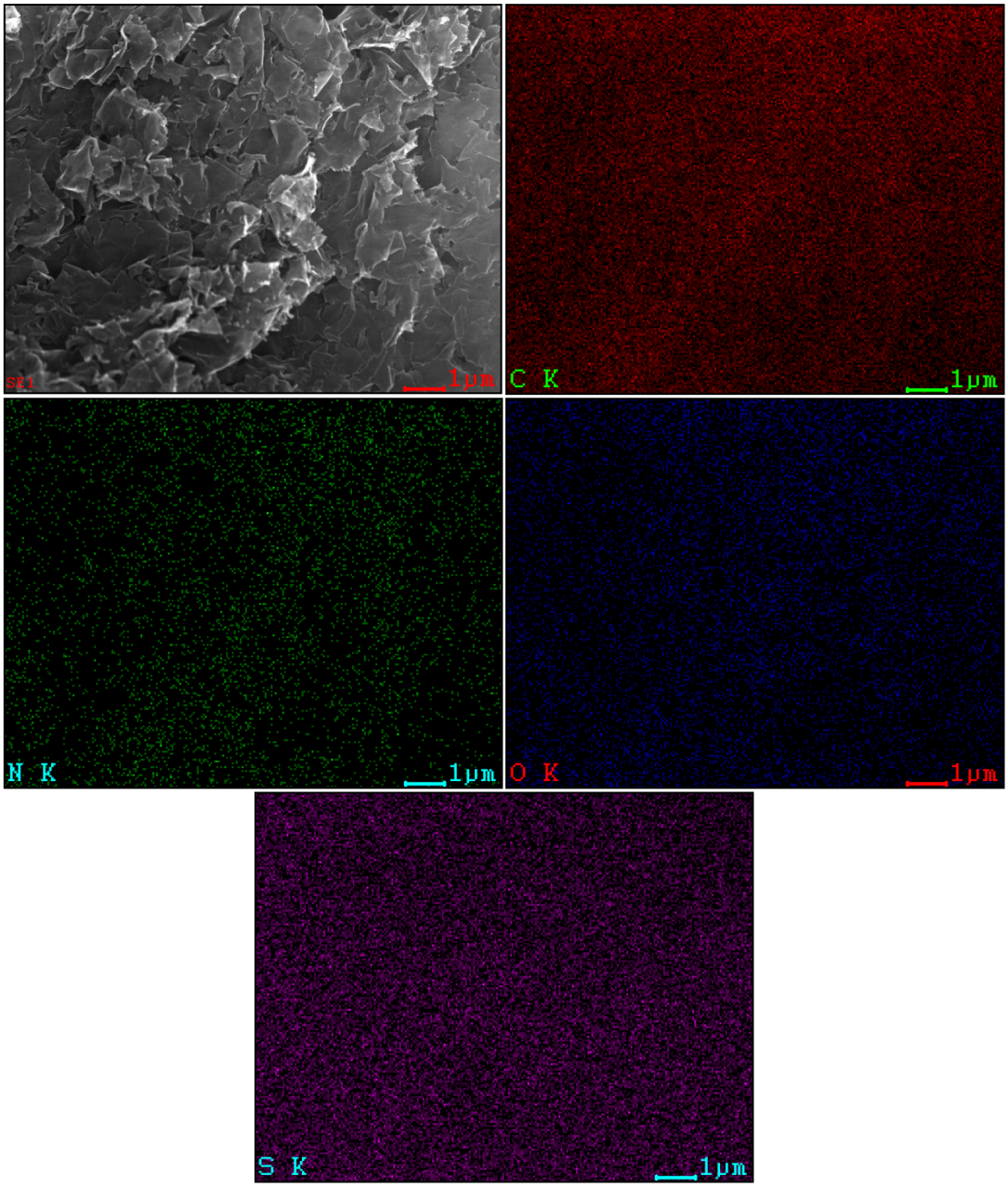

Fig. S8 SEM image of PPy/RGO-10 and the corresponding elemental mapping images for each element.

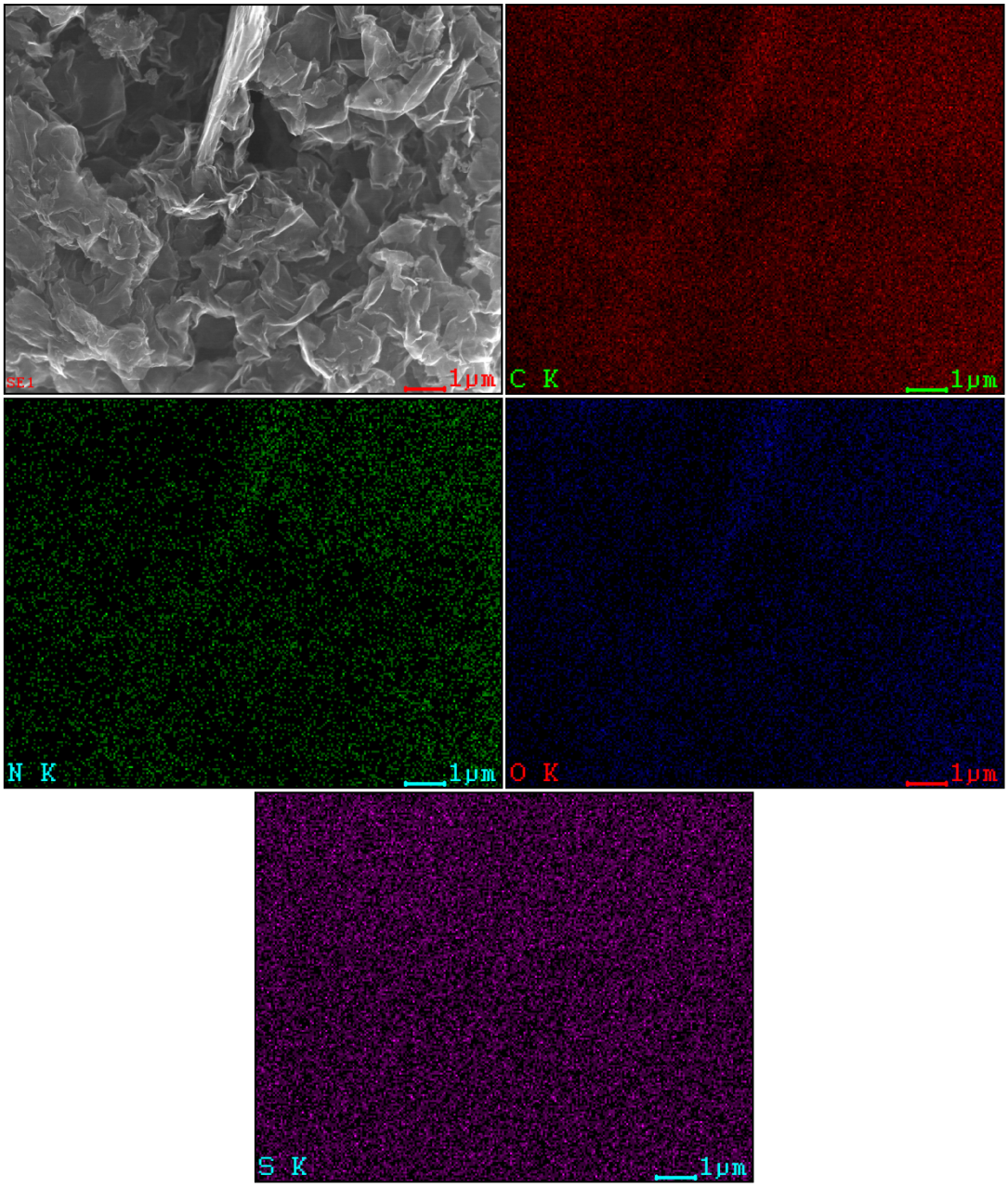

Fig. S9 SEM image of PPy/RGO-10 and the corresponding elemental mapping images for each element.

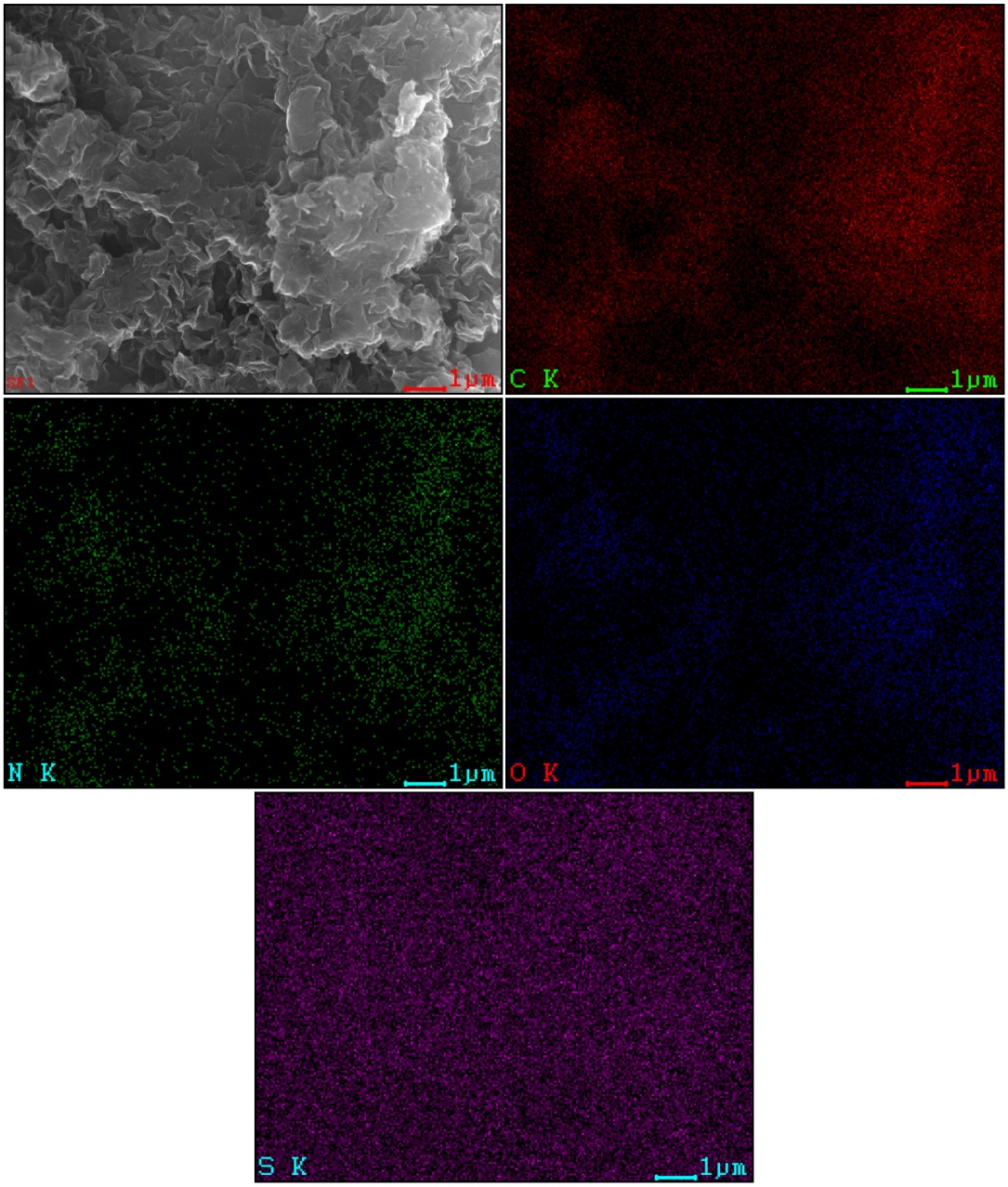

Fig. S10 SEM image of PPy/RGO-20 and the corresponding elemental mapping images for each element.

5. Thermo-gravimetric analysis

the percentage of RGO in the PPy/RGO composites were calculated for the mass loss of each TG curve from 50 to 1000 ℃. Here, we assume that the mass loss of PPy/RGO is equivalent to the mass loss of RGO and PPy at the high temperature up to 1000 ℃. And the results are listed in Table S3.

Table S3 Mass loss and the corresponding percentage of RGO for each PPy/RGO composite.

Sample	the mass loss	the percentage of RGO	Calculated by weighing
PPy	55.99%	0	0
PPy/RGO-2.5	55.03%	2.11%	2.18%
PPy/RGO-5	53.69%	5.28%	5.01%
PPy/RGO-10	51.72%	10.2%	9.62%
PPy/RGO-20	47.86%	19.2%	18.18%
RGO	14.18%	100%	100%

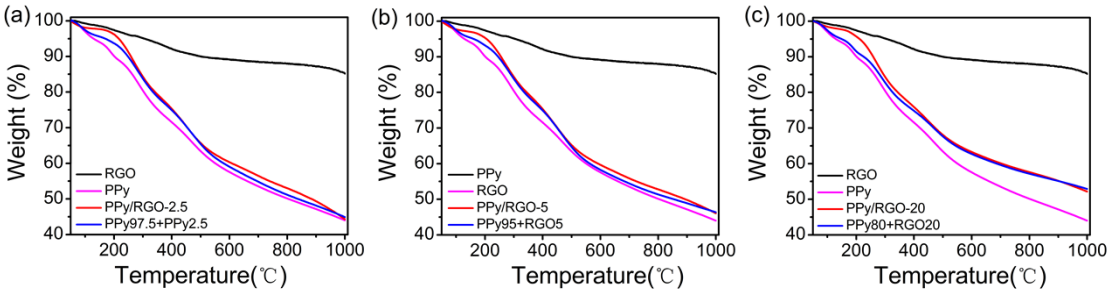

Fig. S11 TGA curves of PPy/RGO-2.5, PPy/RGO-5, PPy/RGO-20, and the samples of physically mixed PPy and RGO at corresponding mass ratios.

6. EIS analysis and calculation of diffusion coefficient

To evaluate the ion diffusion in PPy/RGO-10 and PPy/RGO-20, Fig. S11 shows EIS analiysis of the electrodes at open circuit voltage (OCV) from 10 mHz to 100 KHz. Large charge transfer resistance (R_{ct}) of the PPy/RGO-20 electrode indicates its hindrance for counter-ions diffusion at the electrode/electrolyte interface. And the

Warburg coefficient (σ_w) can be obtained from the plots in the medium frequency region accordion to the following equation [1]:

$$Z_{re} = R_s + R_{ct} + \sigma_w \omega^{-0.5} \quad (1)$$

where R_s is the resistance of the electrolyte and current collector, R_{ct} is the charge transfer resistance and ω is the angular frequency in the medium frequency region. As shown in Fig S11b, the slope of the fitted line is the Warburg coefficient. It is observed that the σ_w of PPy/RGO-10 and PPy/RGO-20 are 0.426 and 1.4 Ω cm^2 s$^{-0.5}$, respectively, which imply that excessive RGO adding into the PPy matrix will hinder the migration of ions and increase the diffusion resistance.

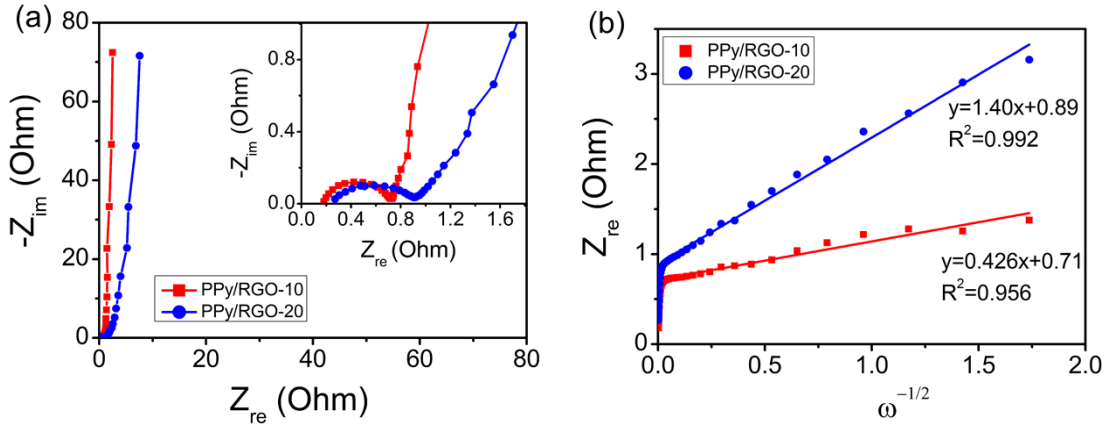

Fig. S12 EIS analysis and the corresponding relationship between Z_{re} and $\omega^{-0.5}$ at middle frequencies for PPy/RGO-10 and PPy/RGO-20 electrodes.

7. Calculation of power and energy density

The power of each device was calculated from the galvanostatic curves at different charge/discharge current densities [2] using the formula given in Equation (2):

$$P = \frac{1}{2} i \times \Delta U \times 1000 \quad (2)$$

Where P is the power density (W kg^{-1}), i is the current density (A g^{-1}), and ΔU is the

operating voltage window (measured in volts and obtained from the discharge curve excluding the *IR* drop (U_{drop}), $\Delta U=U-U_{drop}$).

The energy density of the device was obtained from the formula given in Equation (3):

$$E = \frac{1}{2} \times \frac{C_m}{4} \times \Delta U^2 \Big/ 3.6 \quad (3)$$

Where E is the energy density in Wh kg^{-1}, C_m is the mass specific capacitance (F g^{-1}) and ΔU is the operating voltage window in volts.

And, the *IR* drop (U_{drop}) of each device was shown in Figure S5, which is measured under the same dynamic conditions from galvanostatic curves. Moreover, the R_{ESR} is defined such that $R_{ESR}=U_{drop}/2i$, which is the internal resistance of the device. For the curve of U_{drop} vs. i, the slope is equal to twice R_{ESR}.

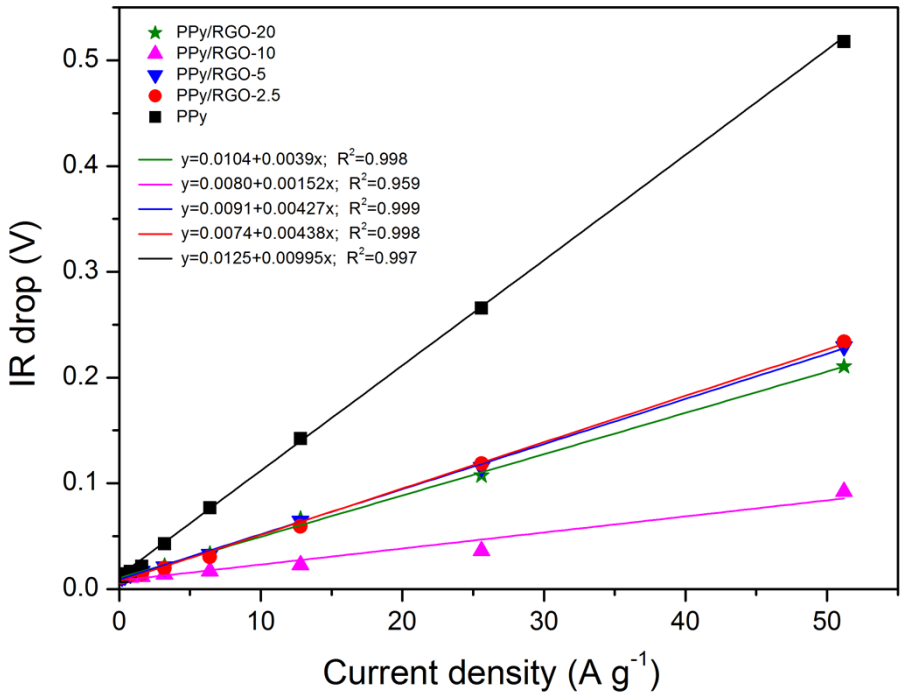

Fig S13 *IR* drop of for PPy and all PPy/RGO composites at different current densities.

References:

[1] A. J Bard, L. R. Faulkenr, electrochemical Methods Fundamentals and Applications, 2nd Edition, John Wiley & Sons, 2001.

[2] Conway, B. E., Electrochemical supercapacitors: scientific fundamentals and technological applications. Kluwer Academic/Plenum Pulishers,1999.